The GEO-SEQ Project
Quarterly Status and Cost Report
March 1, 2001 – May 31, 2001

Project Overview:

The purpose of the GEO-SEQ project is to establish a public-private R&D partnership that will:

- Lower the cost of geologic sequestration by
  (1) Developing innovative optimization methods for sequestration technologies with collateral economic benefits (such as enhanced oil recovery (EOR), enhanced gas recovery (EGR), and enhanced coalbed methane production)
  (2) Understanding and optimizing trade-offs between CO_2 separation and capture costs, compression and transportation costs, and geologic sequestration alternatives.

- Lower the risk of geologic sequestration by
  (1) Providing the information needed to select sites for safe and effective sequestration
  (2) Increasing confidence in the effectiveness and safety of sequestration through identifying and demonstrating cost-effective monitoring technologies
  (3) Improving performance-assessment methods to predict and verify that long-term sequestration practices are safe, effective, and do not introduce any unintended environmental effects.

- Decrease the time to implementation of geologic sequestration by
  (1) Pursuing early opportunities for pilot tests with our private sector partners
  (2) Gaining public acceptance.

Technical work began in May 2000 with an initial focus on four tasks: (A) development of sequestration co-optimization methods for EOR, depleted gas reservoirs, and brine formations; (B) evaluation and demonstration of monitoring technologies for verification, optimization, and safety; (C) enhancement and comparison of computer-simulation models for predicting, assessing, and optimizing geologic sequestration in brine, oil and gas, and coalbed methane formations; and (D) improvement of the methodology and information available for capacity assessment of sequestration sites. Work continued on these four tasks during the fourth quarter. Technical progress and accomplishments are discussed below.

Highlights:

- A new real gas properties module, GasEOS, was implemented in the TOUGH2–EOSTC reservoir simulator to improve numerical simulations supporting assessment of carbon sequestration EGR.
- Reaction-progress-chemical thermodynamic and kinetic simulations show that small amounts of SO_2 in the CO_2 waste stream results, over the long-term, in increased levels of carbon remaining in solution in the formation waters.

- A post-CO_2 injection data set was collected using crosswell seismic and electromagnetic geophysical techniques at the Chevron Lost Hills, California, pilot test site.
- A complementary field program was planned for the Texaco Vacuum Field to test crosswell electromagnetic and electrical-resistance tomography methods.
- The temperature dependence of stable carbon and oxygen isotope partitioning between CO_2 and representative geological materials can vary considerably, depending on whether the solid contains hydrocarbons.
- An updated definition of formation storage capacity was developed that consists of the product of four factors: intrinsic capacity, geometric capacity, heterogeneity, and porosity.

Papers Published and Presented:

Newmark, R.L., A. Ramirez, and W. Daily, "Monitoring carbon dioxide sequestration using electrical resistance tomography (ERT): Sensitivity studies," paper presented and to be published in Proceedings of First National Conference on Carbon Sequestration, Washington, DC, May 14—17, 2001.

Pruess, K., T. Xu, J. Apps, and J. Garcia, "Numerical modeling of aquifer disposal of CO_2," Paper SPE-66537, Presented at SPE/EPA/DOE Exploration and Production Environmental Conference, San Antonio, TX, February 2001.

Pruess, K., C.F. Tsang, D.H.-S. Law, and C.M. Oldenburg, "An intercomparison study of simulation models for geologic sequestration of CO_2," presented and to be published in Proceedings of First National Conference on Carbon Sequestration, Washington, DC, May 14—17, 2001.

Orr, L. and A. Kovscek, "Increasing CO_2 storage in oil recovery," presented and to be published in Proceedings of First National Conference on Carbon Sequestration, Washington, DC, May 14—17, 2001.

Oldenburg, C.M., S.M. Benson, and K. Pruess, "Carbon sequestration with enhanced gas recovery: Identifying candidate sites for pilot study," presented and to be published in Proceedings of First National Conference on Carbon Sequestration, Washington, DC, May 14—17, 2001.

Law, D.H.-S., B. van der Meer, and W. Gunter, "Comparison of numerical simulators for greenhouse gas storage in coalbeds, Part I: Pure carbon dioxide injection," presented and to be published in Proceedings of First National Conference on Carbon Sequestration, Washington, DC, May 14—17, 2001.

Knauss, K.G., J.W. Johnson, C.I. Steefel, and J.J. Nitao, "Evaluation of the impact of CO_2, aqueous fluid, and reservoir rock interactions on the geologic sequestration of CO_2, with special emphasis on economic implications," presented and to be published in Proceedings of First National Conference on Carbon Sequestration, Washington, DC, May 14—17, 2001.

Carroll, S.A. and K.G. Knauss, "Experimental determination of Ca-silicate dissolution rates: A source of calcium for geologic CO_2 sequestration," presented and to be published in Proceedings of First National Conference on Carbon Sequestration, Washington, DC, May 14—17, 2001.

Johnson, J.W., J.J. Nitao, C.I. Steefel, and K.G. Knauss, "Reactive transport modeling of geologic CO_2 sequestration in saline aquifers: The influence of intra-aquifer shales and the relative effectiveness of structural, solubility, and mineral trapping during prograde and retrograde sequestration," presented and to be published in Proceedings of First National Conference on Carbon Sequestration, Washington, DC, May 14-17, 2001.

Rau, G.H., K. Caldeira, K.G. Knauss, W. Downs, and H. Sarv, "Enhanced carbonate dissolution as a means of capturing and sequestering carbon dioxide," presented and to be published in Proceedings of First National Conference on Carbon Sequestration, Washington, DC, May 14—17, 2001.

Hovorka, S.D., C. Doughty, P.R. Knox, C.T. Green, K. Pruess, and S.M. Benson, "Evaluation of brine-bearing sands of the frio formation, upper Texas Gulf Coast, for geologic sequestration of CO_2," presented and to be published in Proceedings of First National Conference on Carbon Sequestration, Washington, DC, May 14—17, 2001.

Doughty, C., K. Pruess, S.M. Benson, S.D. Hovorka, P.R. Knox, and C.T. Green, "Capacity investigation of brine-bearing sands of the frio formation for geologic sequestration of CO_2," presented and to be published in Proceedings of First National Conference on Carbon Sequestration, Washington, DC, May 14—17, 2001.

Cole, D.R., J. Horita, and D.J. Wesolowski, "Fundamental studies of stable isotope exchange in systems relevant to energy utilization," abstract presented at 11th Annual Goldschmidt Conference, Hot Springs, VA, 2001.

Benson, S.M. and L. Myer, "Identifying and addressing key issues in geologic sequestration," abstract presented at 11th Annual Goldschmidt Conference, Hot Springs, VA 2001.

Task Summaries

Task A: Develop Sequestration Co-Optimization Methods

Subtask A-1: Co-optimization of carbon sequestration and EOR and EGR from oil reservoirs.

Accomplishments:

- A preliminary assessment of oil and gas reservoirs and their potential for sequestration of carbon dioxide was completed.

Summary:

The objectives of this subtask are (1) to assess the feasibility of co-optimization of CO_2 sequestration and EOR and (2) to develop techniques for selecting the optimum gas composition for injection. Results will lay the groundwork necessary for rapidly evaluating the performance of candidate sequestration sites as well as monitoring the performance of CO_2 EOR.

The initial focus has been to assess the feasibility of CO_2 sequestration in depleted or inactive oil reservoirs. Existing CO_2– EOR selection criteria have been examined in light of the need to maximize CO_2 storage in a reservoir and the new criteria developed.

Progress This Quarter: Work continued on a report entitled "Criteria for Selecting Oil Reservoirs Suitable for CO_2 Sequestration."

Work Next Quarter: We will work to develop an operational model for simultaneous EOR and sequestration that maximizes ultimate oil recovery and placement of CO_2 into reservoirs for carbon sequestration.

Subtask A-2: Feasibility assessment of carbon sequestration with enhanced gas recovery (CSEGR) in depleted gas reservoirs.

Accomplishments:

- A new real- gas-properties module, GasEOS, was implemented into the reservoir simulator TOUGH2-EOS7C.

Summary:

The objectives of this subtask are to assess the feasibility of injecting CO_2 into depleted natural gas reservoirs for (1) sequestering carbon and (2) enhancing methane (CH_4) recovery. Investigation will include assessments of (1) CO_2 and CH_4 flow and transport processes, (2) injection strategies that retard mixing, (3) novel approaches to inhibit mixing, and (4) identification of candidate sites for a pilot study.

Initial feasibility was assessed through numerical simulation of CO_2 injection into a model system based on the Rio Vista gas field in California. Positive results of this assessment have led to scoping studies for a CSEGR pilot. Industrial partners are now being sought.

In a parallel effort, the numerical simulation capability supporting this assessment is being improved through enhancement to the TOUGH2-EOS7C code.

Progress This Quarter: The new real-gas-properties module GasEos was implemented in TOUGH2-EOS7C. The module modifies gas-mixture densities and enthalpies using the Peng-Robinson equation of state. GasEos was verified by comparison with available published data and other equations of state for the system H_2O-CO_2-CH_4 as shown in Figure 1. Agreement for compressibility factor, density, and enthalpy departure was within 5% for all cases examined. An example of the comparison for the ternary system is shown in Figure 2. Values of the compressibility factor Z are plotted against pressure for various equilibrium gas mixtures consisting of H_2O, CH_4, and CO_2 at two different temperatures.

In other code-development activity, testing began of an implementation of the Dusty Gas Model in TOUGH2 for gas-phase transport.

Finally, efforts continued toward the goal of developing a CSEGR pilot. A talk was presented at the monthly meeting of the Sacramento Petroleum Association in Sacramento, California. Several candidate sites, including gas storage projects, were identified for follow-up discoveries.

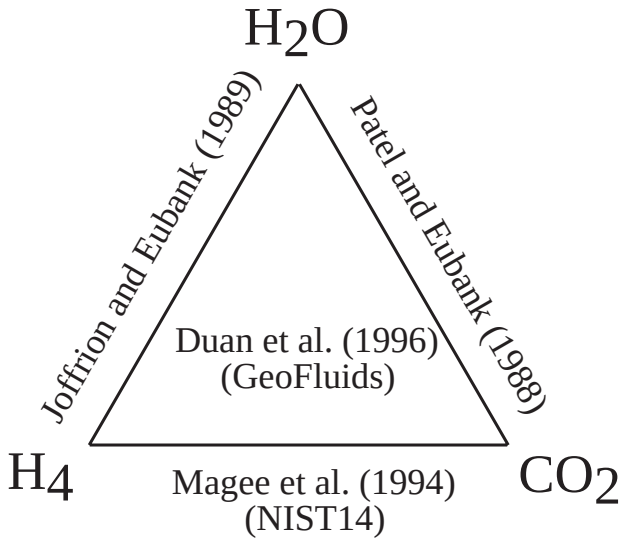

Figure 1. Ternary system H_2O-CO_2-CH_4 and published data or models for the end-member binary systems (Joffrion and Eubank, 1989; Patel and Eubank, 1988; Magee et al., 1994; NIST, 1992) and full ternary (Duan et al., 1996).

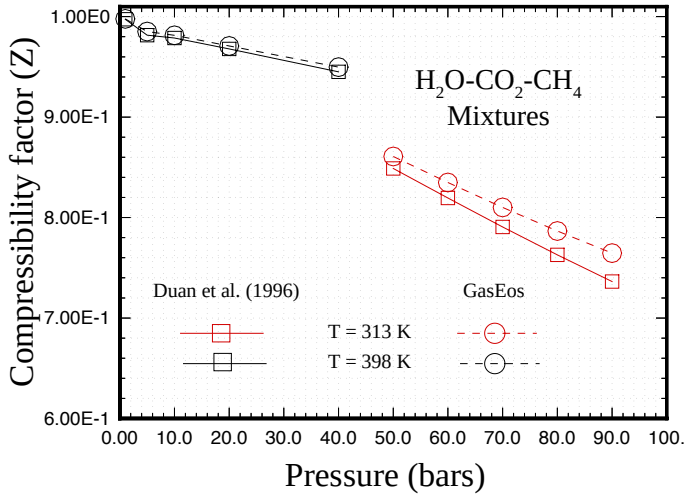

Figure 2. Comparisons of GasEos against Duan et al. (1996) for mixtures in the ternary system H_2O-CO_2-CH_4.

Work Next Quarter: Effort will continue toward identifying a CSEGR pilot site. An economic analysis of CSEGR will be initiated. Simulation studies of CSEGR at high reservoir pressures will be carried out. Implementation and testing of the Dusty Gas Model in TOUGH2 – EOS7C will continue.

Subtask A-3: Evaluation of the impact of CO_2 aqueous fluid and reservoir rock interactions on the geologic sequestration of CO_2, with special emphasis on economic implications.

Accomplishments:

- Reaction-progress-chemical thermodynamic and kinetic simulations show that small amounts of SO_2 in the CO_2 waste stream resulted in much more carbon remaining in solution after 500 years. Addition of H_2S had little impact on sequestering processes.

Summary:

Numerical simulations are being carried out to evaluate geochemical changes accompanying injection of a waste stream containing SO_2, NO_2, and H_2S. Simulations are equivalent to batch-type (closed system) reactions, including full-dissolution kinetics (e.g., acid catalysis) for all of the mineral phases present in the reservoir rock. A rock composition is used with modal abundances appropriate for a feldspathic-sandstone reservoir (containing clay and carbonate with and without a Fe-bearing phase), and a carbonate reservoir (comprised of calcite, dolomite, and siderite).

Progress This Quarter: During this fourth quarter, work continued on the process of evaluating the impact of waste stream contaminants (e.g., SO_2, NO_2, and H_2S) on injectivity and sequestration performance. A series of simulations was constructed that are equivalent to batch-type (closed system) reactions, including full dissolution kinetics (such as acid catalysis) for all of the mineral phases present in the reservoir rock. A rock composition and modal abundances are used that are appropriate for a feldspathic-sandstone reservoir containing clay and carbonate with and without a Fe-bearing phase, and a carbonate reservoir comprised of calcite, dolomite, and siderite.

As an example of the results obtained, a simulation is described of the reaction of a brine that was initially equilibrated with a gas phase consisting of 80 b CO_2 and 10^{-6} b SO_2, that is then allowed to react with the feldspathic sandstone reservoir in isolation from that gas phase at 60°C. Note that this low SO_2 fugacity, when equilibrated with water, is sufficient to drive the pH to a low value (pH = 0.4), because it is readily converted to the strong acid H_2SO_4. In this simulation, it was assumed that in the short-term redox disequilibria would pertain, so effectively all redox reactions are turned off (with the exception of the aqueous oxidation of sulfite to sulfate). The initial fO_2, while low (log fO_2 = -55, approximately equivalent to initial buffering by hematite-siderite), is still just high enough that sulfate is the dominant form of dissolved sulfur. The results during 500 years of reaction are presented in Figure 3.

Notice that in this simulation (Figure 3) the reservoir rock carbonate minerals (calcite and, to a much lesser extent, siderite) react rather quickly with the dissolved CO_2, raising the pH until the carbonate minerals are essentially equilibrated with the resulting solution. The existing carbonate minerals are not sequestering the waste stream CO_2 in this case; indeed, they are adding CO_2 to the system. Because it is a closed-system calculation, the CO_2 fugacity rises from the initial 80 b to 108 b, and so CO_2 (aq) rises from 1.32 to 1.78 m as 88% of the calcite dissolved after approximately 1 day. The pH at this point has risen to 3.97 from the initial 0.4 value. The only form of sequestration at this point is the CO_2 present in dissolved form in solution. From this point forward in the calculation, the principal reaction involves dissolution of the K-feldspar at the still acid pH. However, the Al released from the K-feldspar combines with Na from the brine and dissolved CO_2 to form the mixed hydroxycarbonate mineral dawsonite. This new secondary mineral is sequestering CO_2 via mineral trapping. The silica released from the dissolving K-feldspar is precipitated as the silica polymorph chalcedony, as well as going into growth of additional quartz. Notice that the absolute abundance of quartz is so much larger than the other minerals that we have not plotted it. It grows in linearly at a rate determined by its kinetic rate law, increasing in volume from 1804 cm^3 to 1837 cm^3 after 500 years. The chalcedony and dawsonite both grow in at a rate determined by the dissolution rate of the K-feldspar.

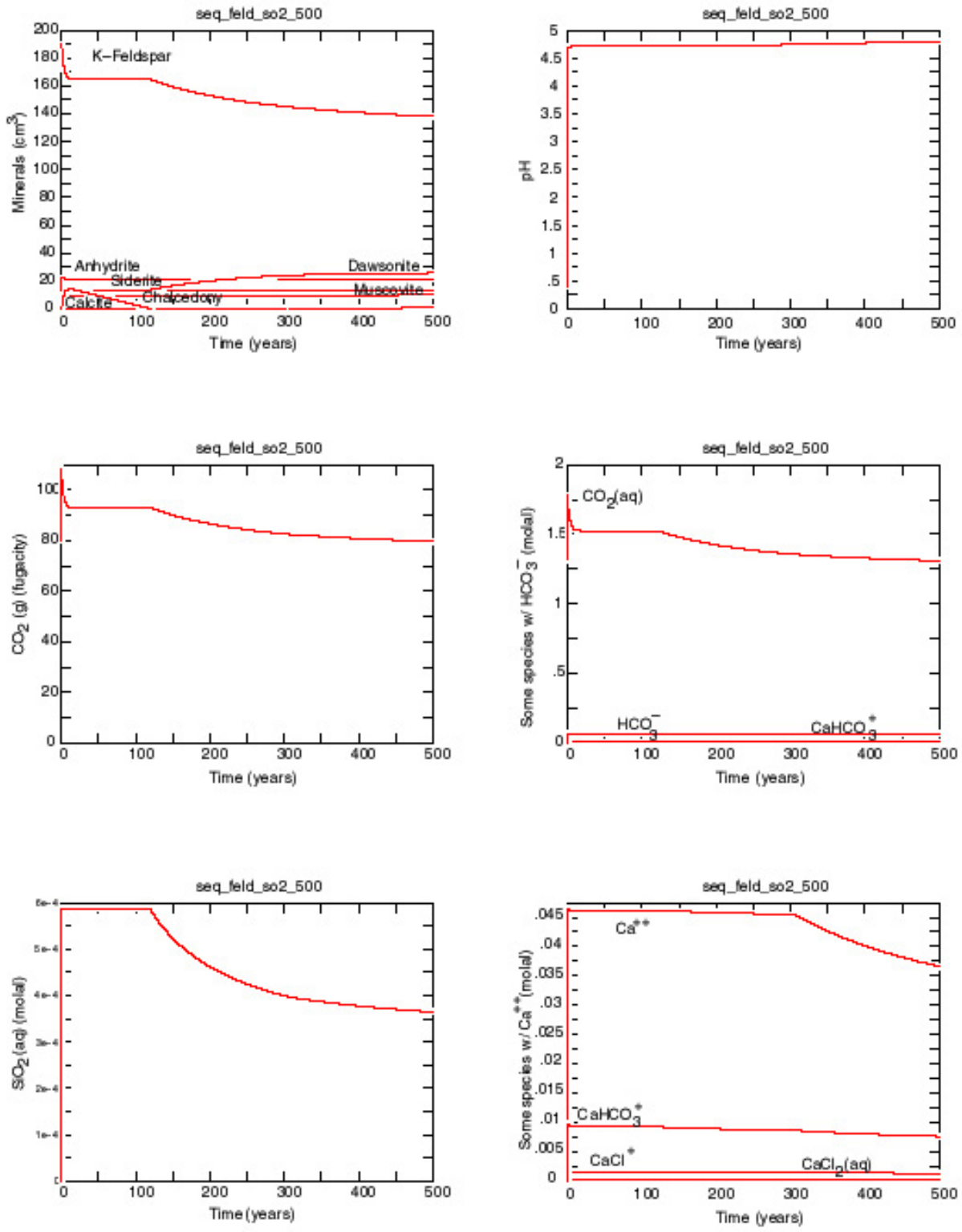

Figure 3. Effects of adding SO_2 to CO_2 waste stream.

The dissolved silica in the simulation maintains a steady-state concentration reflecting the sum of the processes: K-feldspar dissolution quartz precipitation, and chalcedony precipitation. After 12 years or so, the K-feldspar approaches equilibrium with the solution and stops dissolving. After this point, the chalcedony starts dissolving at a rate determined by quartz growth until after 120 years when it is completely consumed. Quartz keeps growing and lowers the dissolved silica to the point that K-feldspar starts dissolving again, allowing more dawsonite to form, sequestering more dissolved CO_2. Note that the pH also increases slightly at the point that the chalcedony disappears, allowing additional calcite to precipitate, also sequestering more dissolved CO_2. By the end of the run at 500 years, quartz is only slightly supersaturated and its rate of growth has slowed considerably. The CO_2 concentration in solution starts out at 1.32 m following the initial equilibration with the gas phase, rises to 1.78 m as the bulk of the calcite dissolves while neutralizing the pH, and then decreases to 1.31 m after 500 years.

To illustrate the impact of SO_2 more clearly, we show in Figure 4 the total number of moles of C in the fluid in equivalent calculations, made with several equilibrating gas-phase compositions: 80 b CO_2, 80b CO_2 and 10 b H_2S, and 80 b CO_2 and 10^{-6} b SO_2. Although the same sequestering processes are occurring in each of the 3 runs, the results are dramatically different in the case of SO_2. Even though the net amount of CO_2 sequestered as the mineral dawsonite after 500 years increases when the acid gases are added (0.400 moles with CO_2, 0.401 moles with CO_2, & H_2S, and 0.437 moles with CO_2 and SO_2), the amount of CO_2 remaining in solution after 500 years is essentially equal to the starting amount when SO_2 is present. This results from the dissolution of nearly all the calcite initially in the rock as the sulfuric acid is neutralized. Recall that the pH of the fluid, after the initial equilibration with the gas phase in the absence of rock, is 3.01 (CO_2), 2.98 (for CO_2 and H_2S), and 0.4 (for CO_2 and SO_2). Because H_2S is a much weaker acid than H_2SO_4, it only dissolves a trivial additional amount of the calcite (beyond that due to CO_2 alone).

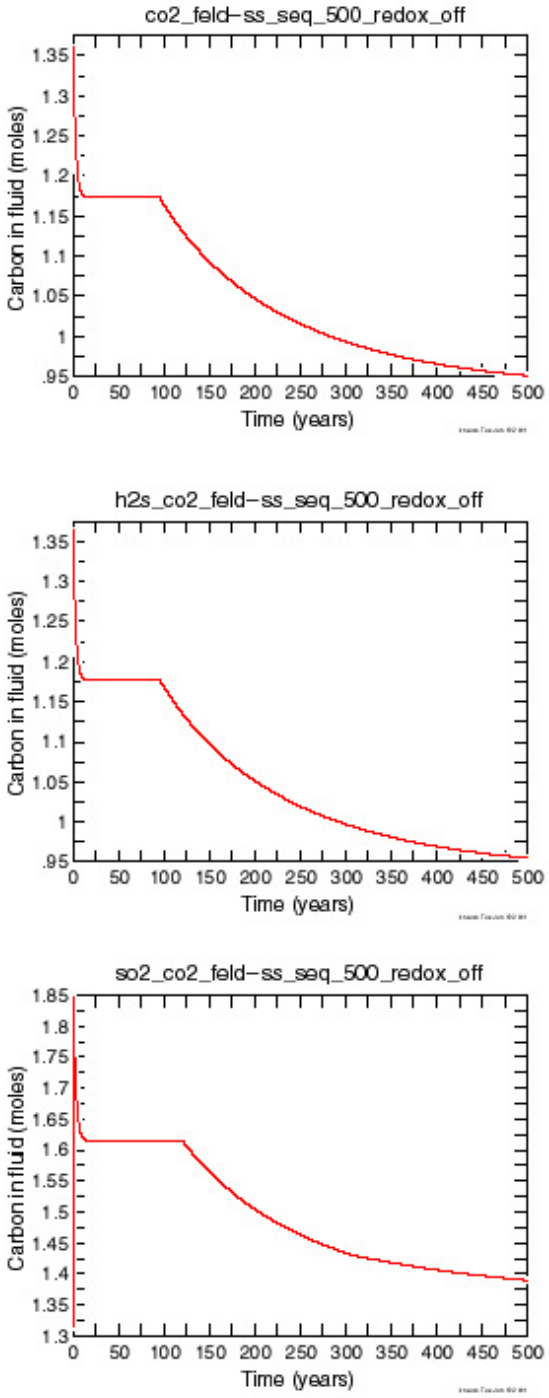

Figure 4. Comparison of the effect of three equilibrating gas phase compositions.

Work Next Quarter: Investigation of the impact of other contaminants (SO_2, H_2S, NO_2, etc.) in the CO_2 will continue. The process of accounting for the impact of fluid flow on sequestration will begin by conducting open-system (reactive transport) calculations analogous to the closed system calculations made to date. The code CRUNCH (Steefel, 2001) will initially be used to make 1D calculations with full chemistry equivalent to all the previous runs.

Task B: Evaluate and Demonstrate Monitoring Technologies

Subtask B-1: Sensitivity modeling and optimization of geophysical monitoring technologies

Accomplishments:

- Reservoir simulations were initiated to predict production and the distribution of fluids in the reservoir resulting from injection of CO_2 at the Chevron Lost Hills field pilot.

Summary:
The objectives of this task are to: (1) demonstrate methodologies for and carry out an assessment of the effectiveness of candidate geophysical monitoring techniques, (2) provide and demonstrate a methodology for designing an optimum monitoring system, and (3) provide and demonstrate methodologies for interpreting geophysical and reservoir data, to obtain high-resolution reservoir images.

The Chevron CO_2 pilot at Lost Hills, California, is being used as an initial test case for developing these methodologies (see Subtask B-2 for background information). Work to date has focused on modeling the geophysical response of seismic and electromagnetic (EM) surveys made before injection of CO_2. The first step in this process was to perform a reservoir simulation (provided by Chevron) of fluid production (oil, water, gas) and fluid injection (water flooding) that took place before and after CO_2 injection. The reservoir model simulations provide estimates of porosity, fluid saturation, pressure, and distribution as a function of lithology in the reservoir. Using well logs and rock physics models, we converted this information to seismic velocities and electrical conductivity. Forward simulations were then performed to generate the seismic wavefield that would be sampled by a crosswell seismic survey and the electrical field that would be sampled by a crosswell EM survey.

In a parallel effort, numerical simulations have also been carried out to access the sensitivity of electrical resistance tomography (ERT) for detection of CO_2. These studies have used models representative of expected conditions at the Hall-Gurny Field, Russell County, Kansas, and the Sleipner project, Norway.

Progress this Quarter: The reservoir model simulation at different times in the CO_2 flood was converted to geophysical parameters as described in our previous reports. The numerical geophysical data generated from these time snapshots were then processed through seismic tomographic and EM inversion routines to produce images of time-lapse changes in electrical conductivity and seismic velocity (for comparison with the changes produced in the flow simulator). Figure 5 shows the electrical-conductivity and seismic-velocity changes from the flow simulation models compared to the changes computed by differencing the images produced by seismic tomography and EM inversion of the simulated data. The vertical areas of largest change indicate the location of the two hydro-frac intervals about 20 ft from the left side of the images. In general, the geophysical difference images do a good job of showing the large-scale changes, both in terms of their spatial extent and their magnitude. The difference images do not show the fracture directly, although there is a slight hint of the fracture locations in the conductivity-difference plots.

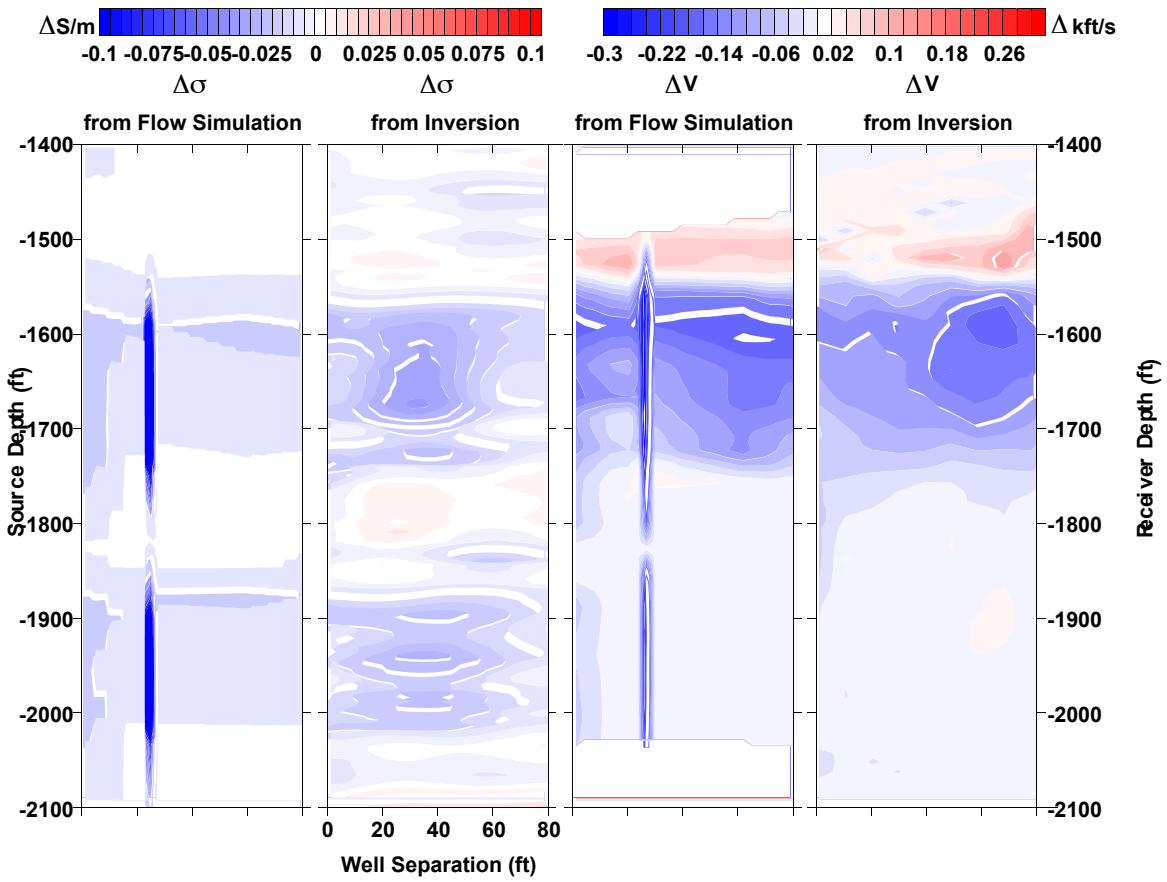

Figure 5. Comparison between actual property changes and imaged property changes from flow simulation model. The first panel on the left is the modeled change in electrical conductivity between April 2001 and September 2000 from differencing flow simulations. The second panel from left is the imaged change in conductivity. The second panel from right is the change in seismic P-wave velocity from differencing flow simulations between May 2001 and September 2000. Panel on right is the change in velocity from differencing tomographic velocity models.

The results established that geophysical data has the potential to accurately map changes in the reservoir on a scale greater than the fractures themselves and provided confidence that geophysical imaging could predict changes in the reservoir, provided that a good model is available to link geophysical parameters to reservoir parameters.

During the first CO_2 injection phase, producing wells unexpectedly began to produce hydro-frac sand. The CO_2 flood was stopped and a brief period of water flooding was carried out to clean the producing wells. Just prior to beginning the short water flood, the two observation wells used for crosswell experiments were re-logged for electrical conductivity. Although no crosswell geophysical experiments were performed at this time, the observed conductivity changes in the wells can be compared to what the reservoir flow simulator predicts. Figure 6 shows the measured differences in log conductivity on either side of the change in electrical conductivity from the flow simulation model. Below 1,580 feet depth the logs show an overall increase in electrical conductivity. The flow simulation model also predicts an increase in conductivity over much of the same interval. In the flow simulation model, the increase in conductivity is associated with an increase in water saturation, which happens when injected CO_2 moves water

in the formation away from the out-of-plane injector into the image plane. The areas of flow simulation that show a decrease in conductivity are associated with an increase in CO_2 saturation. Comparison of the logged changes with the predictions from the flow simulation indicated that the permeability in the vicinity of the OB-C1 well is too high in the model, resulting in the premature presence of CO_2 near the OB-C1 well. Combining rock physics models with the results of the flow simulation indicate that the increase in electrical conductivity is caused by increased water saturation, and that zones that show a decrease in electrical conductivity have CO_2 present.

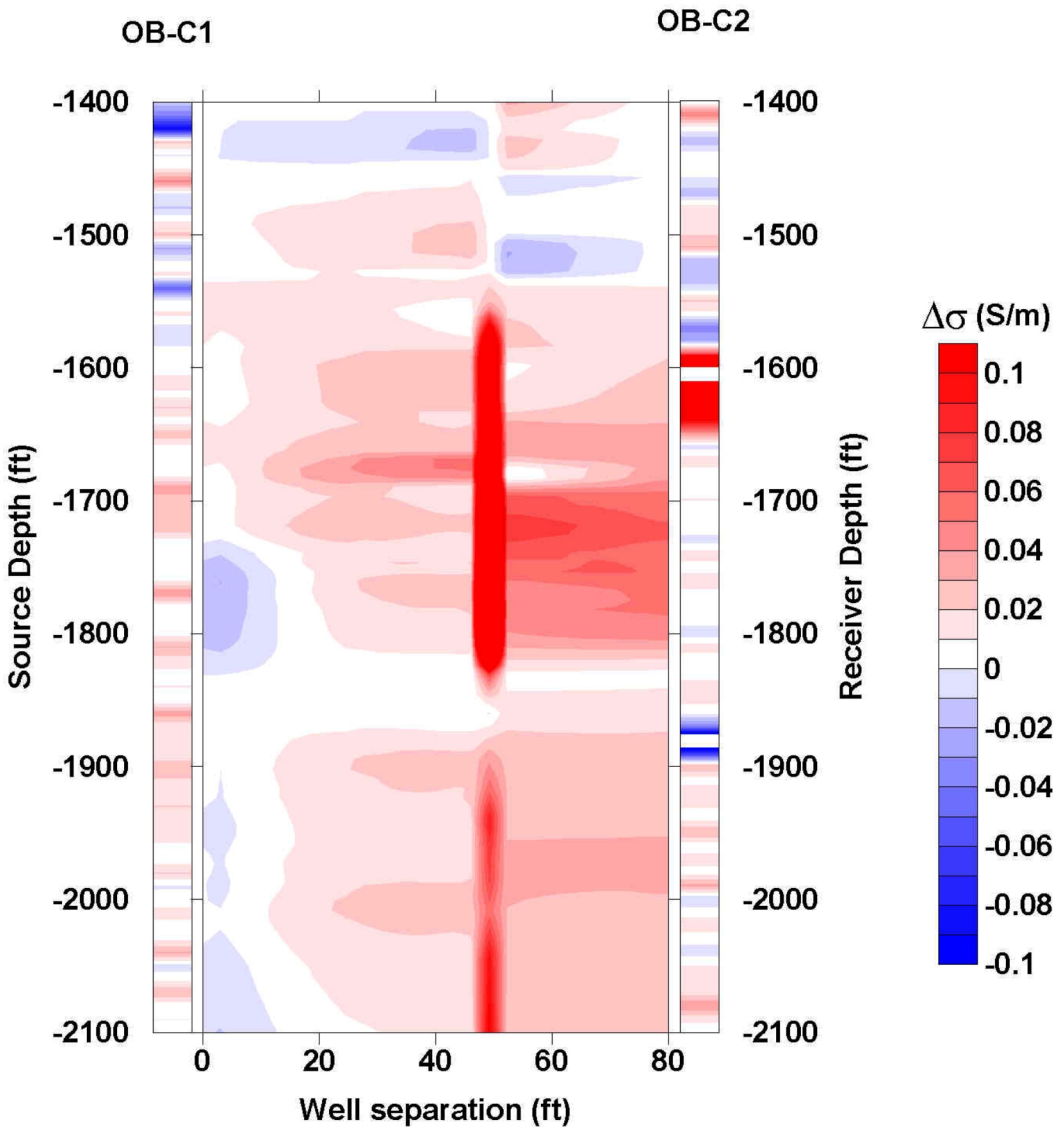

Figure 6. Time difference conductivity logs on either side of the time difference conductivity from the flow simulation model.

The pre- and post-injection data sets were inverted to produce electrical conductivity and seismic-velocity images. These images were differenced (post minus pre) to provide images of the change in geophysical properties. Figure 7 shows these difference images.

In the initial EM inversions, the location of the mapped fault (shown as a red line in Figure 7) corresponded with a transition zone between negative (blue) changes on the left and positive (red) changes on the left. Removing lateral smoothing in the inverse image across the mapped fault location to produce the image shown in Figure 7 sharpened the EM inversion images. The interpretation is that the fault is in some way influencing the flow in the reservoir. While it may not be a strict barrier, it does seem to inhibit flow since the increase in conductivity associated with an increase in water saturation (seen in the re-logging of the wells in January 2000) is still present in April 2001 between the fault and the OB-C2 well.

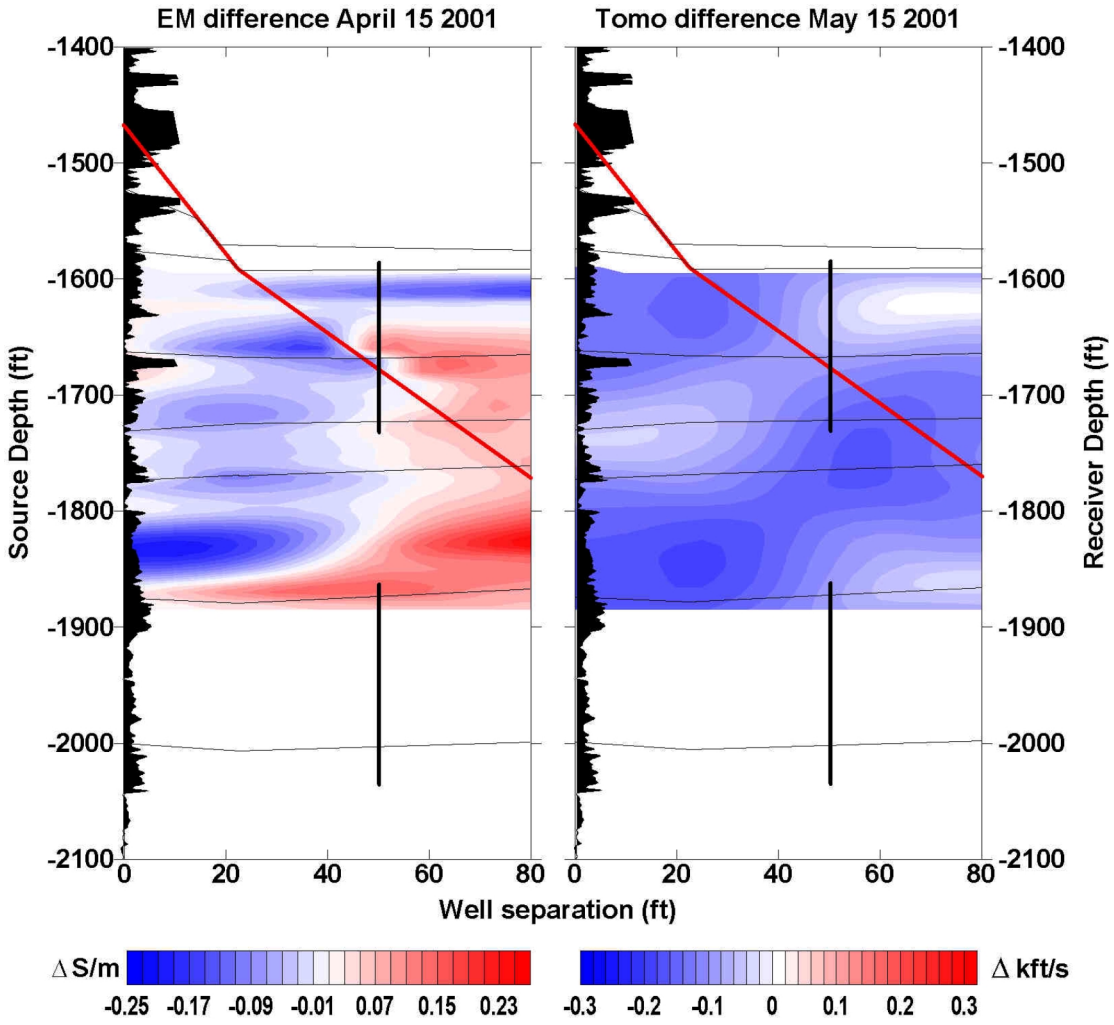

Figure 7. Time-lapse electrical-conductivity and seismic-velocity images from field data. Left panel: Conductivity change between April 2001 and September 2000. Right panel: Velocity change between May 2001 and September 2000. OB-C1 permeability log is displayed on the left side of each image as well as mapped unit boundaries and an interpreted fault in red.

The velocity difference image generally shows a decrease in velocity over the entire image plane, with certain areas showing little or no change. To understand the changes in conductivity in conjunction with those in velocity, a rock physics model must be used.

Time-lapse changes in conductivity are dominated by changes in water saturation. That being the case, conductivity difference images can be used to predict the change in water saturation. If the conductivity changes are used to predict water saturation changes, then the flow simulations can be used to predict pressure changes, and CO_2 changes can be inferred from the velocity changes. A major uncertainty in this procedure is that the pressure change is predicted by the flow simulation model. However, the pressure changes are broadly distributed over the model and are believed to be close to true values. In addition, these will be refined as updated flow simulations are done. Consider three examples in a region where the average effective pressure change is near –1.5 MPa. Figure 8 shows changes in reservoir and geophysical parameters based on the model developed by fitting well log data. This figure is produced at reference values of 50% porosity and a mean effective pressure of 4.4 MPa (taken from the flow simulation in this depth interval 1,400-2,100 ft just prior to CO_2 injection). First, the velocity change is predicted solely from pressure changes.

Figure 8. Left Panel: Change in conductivity (vertical axis) versus change in water saturation (horizontal axis). Right panel: Contours of change in velocity as a function of change in effective pressure (vertical axis) and change in water saturation (horizontal axis). Symbols 1, 2, and 3 mark values taken from the difference images shown in Figure 7 (see text).

Point 1 in Figure 8 represents the conductivity change seen at a depth of 1,850 ft at 20 ft from the OB-C1 well (see Figure 7). This corresponds to a –0.26 change in water saturation. The right panel in Figure 8 shows that this water saturation change (at an effective pressure change of –1.5 MPa) gives a velocity change of –230 ft/s. The observed change in velocity from the image in Figure 7 is –170 ft/s. For point 2 at a depth of 1,700 ft and 20 ft from OB-C1, the model predicts –160 ft/s and –100 ft/s, as observed in Figure 8. For point 3 at a depth of 1,650 ft and 70 ft offset from OB-C1, the model predicts a velocity change of –80 ft/s and –60 ft/s.

The difference between the predicted velocity decrease from changes in effective pressure and the observed velocity decreases can be accounted for by an increase in CO_2 saturation. Figure 9 shows a model-derived change in velocity versus change in effective pressure and change in gas saturation at a water saturation of 0.5. This type of calculation would have to be done for each point to predict the gas saturation change associated with each velocity change, once the change caused by pressure had been removed. This procedure will ultimately be applied to the geophysical images to provide images of water and CO_2 saturation changes.

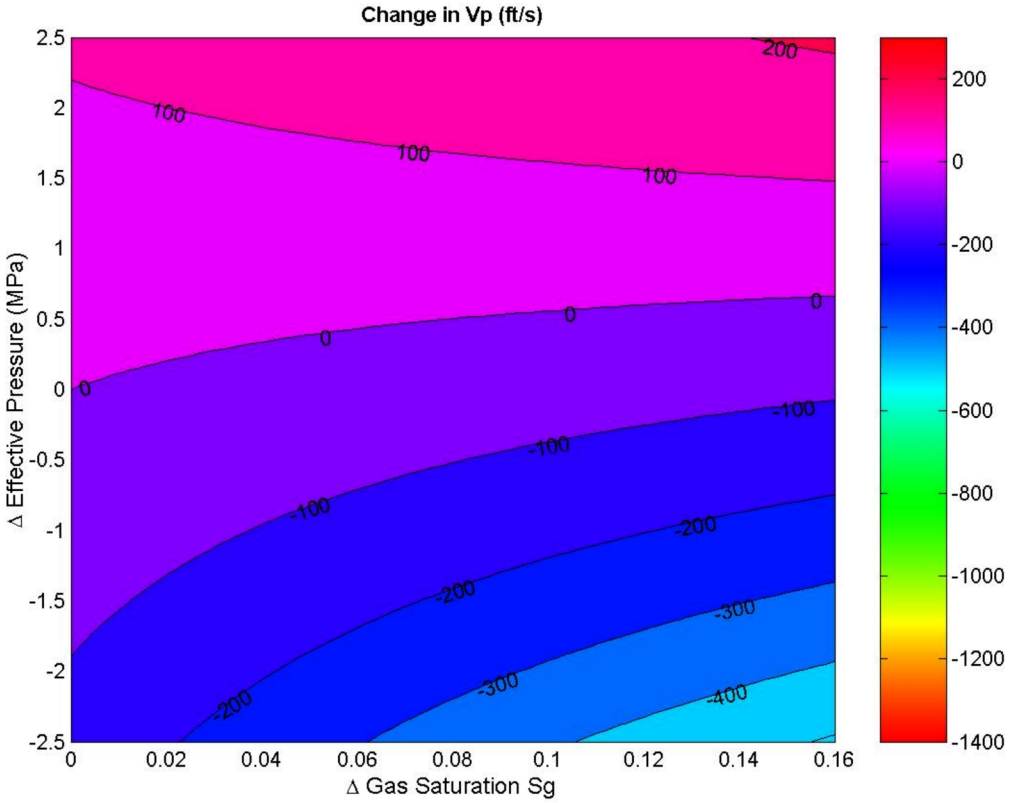

Figure 9. Contours of change in velocity versus changes in effective pressure (vertical axis) and changes in gas saturation (horizontal axis) for reference values of 0.5 water saturation, 4.4 MPa effective pressure.

This analysis is clearly preliminary and dependent on many assumptions, which will be tested and refined as the analysis proceeds. However, all measurements are consistent, and predicted numbers are very close to observed values. Results indicate that the crosswell geophysical imaging is directly sensing the changes in reservoir properties and will allow not only separation of the effects of changes in water and CO_2 saturation from changes in pressure, but will also allow mapping of these changes spatially in far greater detail that is possible from the surface.

Work Next Quarter: Estimates will be made of changes in shear-wave velocity, which if successful will provide an independent data set that will in principal allow estimation of the pressure changes independently from the flow simulation modeling. In addition, the flow simulation model will be refined both in terms of modified permeabilities (as inferred from the geophysical imaging) and incorporating small-scale faulting (as seen in the logs). The flow simulations will be updated to more closely match the observed changes. Once a flow simulation model is derived with improved predictive capabilities, the pressures from this model will be used as illustrated above to convert the difference images into images of change in water saturation and CO_2 saturation. Finally, a single-well seismic-reflection data set is being analyzed in attempt to directly image the fracture location and estimate the fluid saturations within the fracture itself. If this is successful, this information will be incorporated into our EM and seismic inversions to further refine these images.

Subtask B-2: Field data acquisition for CO_2 monitoring using geophysical methods

Accomplishments:

- A post-CO_2 injection data set was collected using crosswell seismic and electromagnetic geophysical techniques at the Chevron Lost Hills, California, pilot test site.
- A field program to obtain both coarse-point electrode and casing ERT surveys in an oil field undergoing CO_2 flood (in conjunction with a commercial crosswell EM survey) was developed.
- Design and construction began of instrumentation capable of obtaining coarse-point electrode data in deep open holes.

Summary:

The goal of this subtask is to demonstrate (through field testing) the applicability of single-well, crosswell, surface-to-borehole seismic, crosswell electromagnetic (EM), and electrical-resistance tomography (ERT) methods for subsurface imaging of CO_2.

The CO_2 injection pilot operated by Chevron USA in Lost Hills, California, provides an early opportunity to test these techniques. This pilot is divided into four injection-centered, 2.5-acre patterns as shown in Figure 10. The figure also provides some interpreted geology for the site. The production interval is from 1,200 ft to 2,100 ft below ground surface, and the CO_2 injection interval is from 1,500 ft to 2,000 ft. The CO_2 injection began in August 2000 at a relatively low flow rate of 125 million cubic feet (Mcf) per day and was gradually increased to 425 Mcf/day per injection well. The injection pressure is being held at 800–900 psi and the reservoir temperature is about 100° F. At these pressure and temperature conditions, the CO_2 is expected to be in gas phase. In early January 2001, CO_2 injection was stopped in the four injection wells because of sanding problems in some of the producing wells. The wells were cleaned out, and CO_2 injection has been restarted in one of the injection wells.

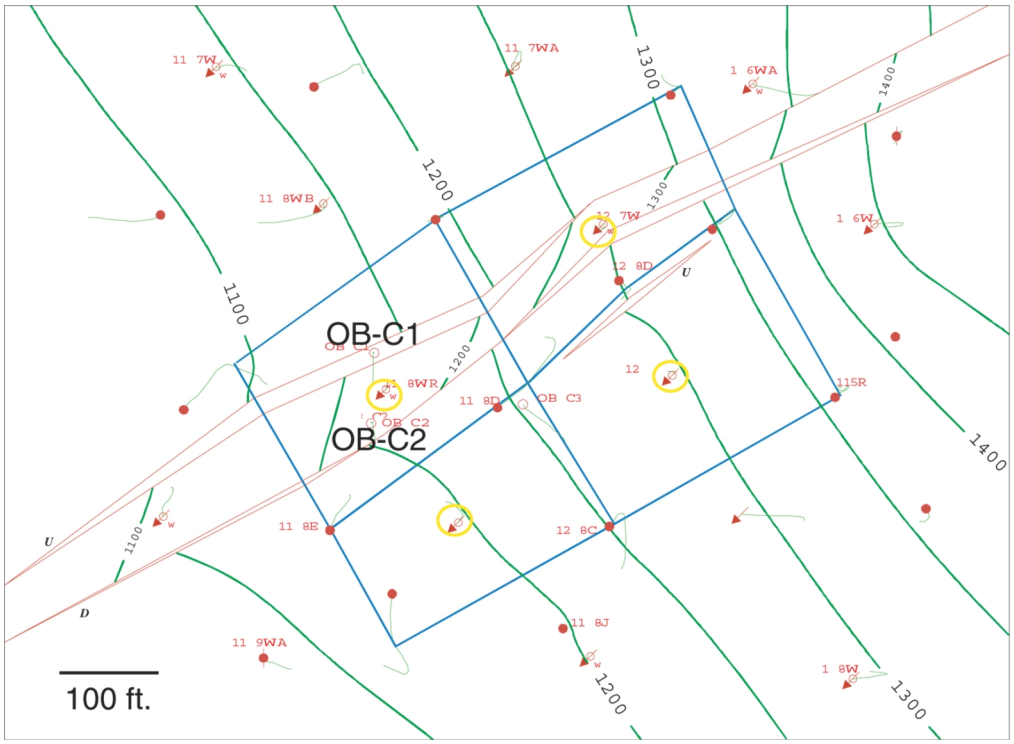

Figure 10. CO_2 injection site (blue lines) with contoured top of reservoir (green lines) and interpreted faults (red lines).

The reservoir volume around injection well 11-8WR is being monitored by high-resolution geophysical techniques. Crosswell seismic and EM measurements were made between observation wells OB-C1 and OB-C2, and single-well seismic measurements were made in OB-C1. Figure 11 provides a time line for the various measurements made in the experiment.

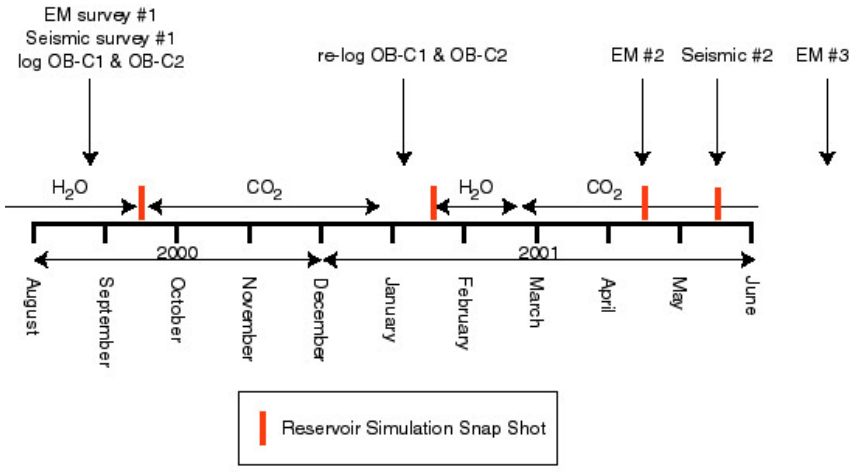

Figure 11. CO_2 injection experiment time line (also showing times of reservoir simulations used in Subtask B-1).

The second EM survey was conducted in mid-April 2001, and the second seismic survey was conducted in May 2001. Note that a third EM survey is planned for late July. This third EM survey will bracket the second seismic survey and provide a means to interpolate the conductivity changes to the same time as the seismic changes.

Progress this Quarter: The data acquired in the post-CO_2 injection seismic surveys included two crosswell surveys, one using a high-frequency (2000 Hz) piezoelectric source with hydrophone sensors, and one using a low frequency (300 Hz) orbital vibrator source (generating both P- and S-waves) with hydrophone sensors. Also acquired were single-well seismic data using the piezoelectric source with hydrophone sensors and the orbital vibrator source with locking 3-component geophones.

To date, the high-frequency crosswell data has been processed and a post-injection P-wave velocity tomogram (Figure 12) generated, as well as a time-lapse velocity change tomogram (Figure 13). Clear changes in velocity can be seen. A simplistic interpretation of the seismic changes seen in Figure 13 would be that the CO_2 concentrations are highest in those regions showing the largest change in seismic velocity. This assumes that the gas-phase CO_2 has decreased the seismic velocity in the post-injection survey. A joint seismic-electromagnetic inversion to constrain reservoir models of CO_2 distribution is being conducted in Subtask B-1. Also note that different color scales are used in Figures 7 and 13.

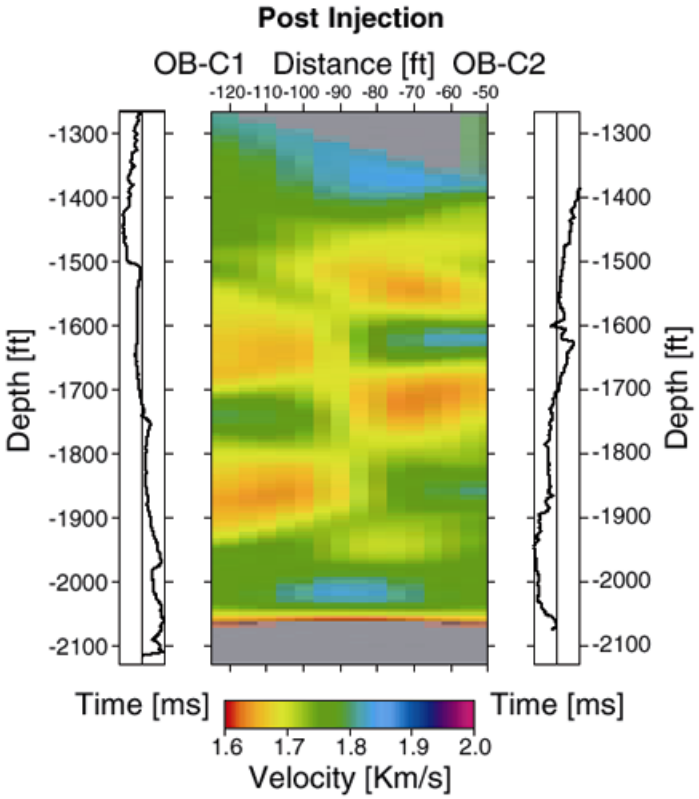

Figure 12. Post-injection seismic-velocity tomogram (center). Borehole static corrections are displayed on either side for the two observation boreholes used (OB-C1 and OB-C2).

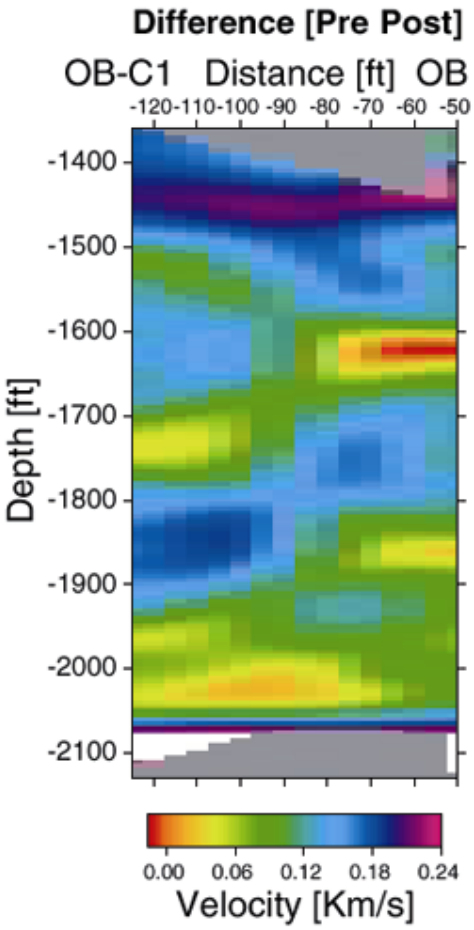

Figure 13. Change in tomographically imaged seismic velocity (pre-injection velocities minus post-injection velocities). While this data will be used in a joint reservoir model inversion, a simplified interpretation is that the largest positive change (blue) indicates the presence of injected CO_2.

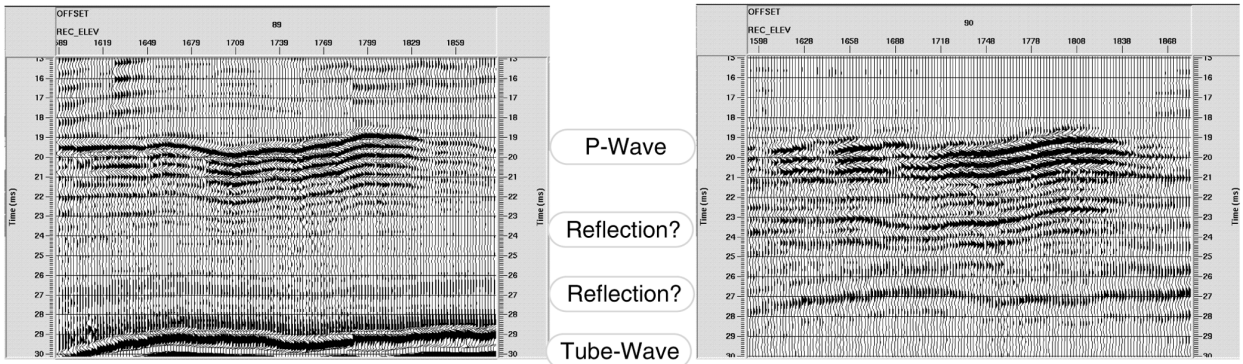

Figure 14. Single-well data from OB-CI pre-injection (left) and post-injection (right). The increase in amplitude of events between the P-wave arrival and the tube-wave arrival indicates that they are possible reflections whose intensity has been increased by the presence of gas-phase CO_2 in the hydrofracture. If true, this would allow direct imaging of the zone containing most of the CO_2 in the subsurface.

Figure 14 shows data from the piezoelectric single-well survey. The dramatic change in tube-wave energy is caused by field deployment of a newly developed tube-wave suppressor.

In a parallel activity, a field program in which electrical/electromagnetic methods would be applied to monitor CO_2 injection was developed. Through interactions with Texaco and EMI (a commercial EM survey company), a joint field program has been developed that will permit both crosswell EM and ERT surveys to be obtained during a CO_2 flood designed for EOR.

The location of this project is Texaco's Vacuum Field in New Mexico. The Vacuum Field was discovered in 1929; however, development did not begin until 1937. Waterflood operations began in the late '60s to '70s, to provide pressure support to the reservoir. CO_2 flood has been initiated in other portions of the field; our field surveys are planned for an area in which Texaco is expanding their CO_2 flood operations. For each subsequent flood program, infill drilling has been conducted. The initial 40-acre spacing has been reduced to 10 acre 5-spots; this presents a poor aspect ratio for high-resolution imaging, but will permit realistic conditions for testing the sensitivity of the methods. Texaco is making available both open and cased holes in the target area.

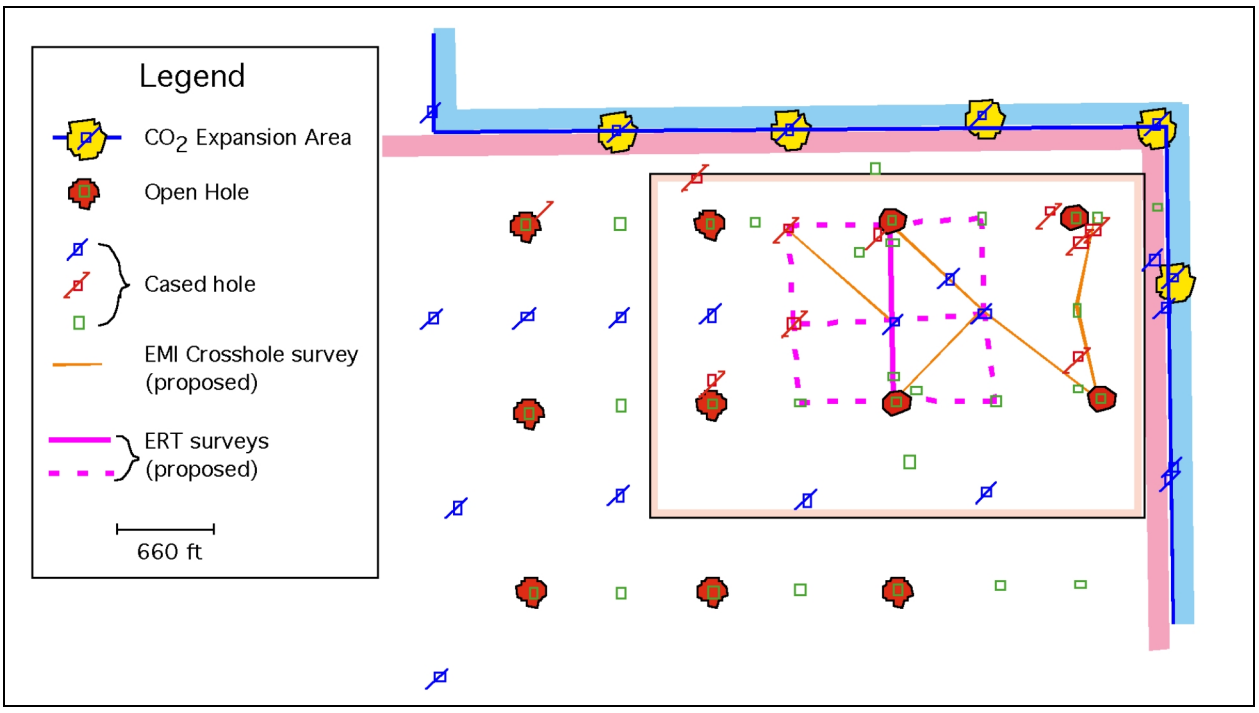

Figure 15. CO_2 expansion project and proposed surveys in Texaco Vacuum Field.

Given this opportunity to access both open and cased holes in the field, both an ERT point-electrode crosswell survey and a casing survey are planned. The coarse-spaced point-electrode crosswell study will permit validation of the range of resistivity changes observed over the operational depth interval and permit direct comparison with EMI's crosshole EM surveys. Our goal is to conduct the ERT field surveys in conjunction with the EMI survey, to minimize overall down time for Texaco's production wells. The work plan is designed to be as seamless and transparent as possible to normal operations. The casing survey is expected to provide

coverage of lateral changes in the reservoir over time for a larger region. The process of constructing the necessary instrumentation to obtain the coarse-point electrode survey is underway.

Work Next Quarter: Work will continue in processing and analyzing the post-injection seismic surveys. This includes processing of the orbital vibrator crosswell and single-well data sets. These results will be integrated into the joint inversion and reservoir model. At the Vacuum Field, initial baseline surveys are planned for late August 2001. Subsequent "time-lapse" surveys would be fielded after sufficient time has elapsed to detect significant changes in the reservoir. The first repeat survey is planned to occur after several months' time (in the January-March 2002 timeframe). Schedules will need to be flexible to accommodate both the needs of the operator and those of EMI, a commercial company.

Subtask B-3: Application of natural and introduced tracers for optimizing value-added sequestration technologies

Accomplishments:

- The temperature dependence of stable carbon and oxygen isotope partitioning between CO_2 and representative geological materials can vary considerably, depending on whether the solid contains hydrocarbons.
- Detailed measurements of surface area and micro-porosity have been completed on a suite of samples used in the isotopic-partitioning experiments.
- Mass-balance isotopic-reaction calculations have been completed indicating that the magnitude and trajectory of change of carbon and oxygen isotopes in CO_2 reacted in the system calcite-CO_2-H_2O can vary markedly, depending on the initial isotopic compositions of the CO_2, H_2O, and $CaCO_3$, the temperature of interaction, and the relative abundance of each constituent.
- Preliminary organic chemical analysis of the Lost Hill core used in the isotopic-partitioning experiments indicates a complex mix of alkylated hydrocarbons, naphthaleness, steroids, and a high water content.

Summary:

The overall goal of this effort is to provide methods that utilize the power of natural and introduced tracers to decipher the fate and transport of CO_2 injected into the subsurface. The resulting data will be used to calibrate and validate predictive models used for (1) estimating CO_2 residence time, reservoir storage capacity, and storage mechanisms; (2) testing injection scenarios for process optimization; and (3) assessing the potential leakage of CO_2 from the reservoir.

To date, work has focused primarily on isotopic tracers. Effort has been directed to accessing carbon and oxygen isotope change as the CO_2 reacts with potential reservoir phases. Both laboratory isotope-partitioning experiments and mass-balance isotopic-reaction calculations have been performed. In addition to investigation of generic rock fluid systems, studies specifically focused on the Chevron Lost Hills CO_2 pilot have also been carried out.

Progress this Quarter: Efforts this quarter have focused on four interrelated activities: (a) investigation of the temperature dependence of C and O isotope partitioning between CO_2 and select geological materials (e.g., quartz, calcite, montmorillonite, Lost Hills core), (b) detailed measurements of surface areas and pore sizes in solids used in isotopic exchange experiments,

(c) mass-balance calculations designed to quantify the magnitude of C and O isotope change during reaction of CO_2 with calcite and H_2O, and (d) preliminary assessment of the organic chemistry of the Lost Hills core used in our experiments.

Carbon and oxygen isotope-partitioning experiments in static systems have been conducted at temperatures of 35°C and 50°C to complement previous 20°C studies. Carbon dioxide of known C and O isotope composition was reacted with various geological materials, and the isotopic difference between free CO_2 and CO_2 absorbed onto the solids was measured. As with our 20°C studies, both C and O isotope values of the free CO_2 with calcite and H_2O, and (d) preliminary assessment of the organic chemistry of the Lost Hills core used in our experiments.

Carbon and oxygen isotope-partitioning experiments in static systems have been conducted at temperatures of 35 and 50°C to complement previous 20°C studies. Carbon dioxide of known C and O isotope composition was reacted with various geological materials, and the isotopic difference between free CO_2 and CO_2 absorbed onto the solids was measured. As with our 20°C studies, both C and O isotope values of the free CO_2 are always enriched in the heavier isotope (^{13}C or ^{18}O) relative to CO_2 absorbed onto mineral surfaces. For crystalline phases such as quartz, calcite, and montmorillonite, the magnitude of this partitioning decreases with increasing temperature at a rate of only a few per mil per 15°C increase in temperature. Isotopic behavior determined for the Lost Hills core was the opposite in effect compared to the crystalline solids. The magnitude of both C and O partitioning increased at a rate of several per mil per 15°C increase in temperature for all four core samples tested. Similar behavior was also observed for the one Lost Hills oil sample also investigated.

These results have two implications for the monitoring of CO_2 during injection testing. First, the temperature dependence of the adsorption process can be ignored for CO_2 interaction with crystalline host lithologies, but not in cases where hydrocarbons are present. Second, the difference in the direction of enrichment between hydrocarbon-bearing and nonhydrocarbon-bearing host rocks as a function of temperature might afford a possible further means to determine what horizons the CO_2 interacted with.

Detailed measurements were carried out on the surface areas and pore sizes of solids used in our adsorption isotope studies, using a newly acquired Quantachrome surface area analyzer. The sorption gas used in all cases was N_2. Five samples were examined: quartz, calcite, montmorillonite, Lost Hills core 4, and Argonne premium coal sample Pocahantus#3. The average measured specific surface areas in m^2/gm are 0.1233, 0.7129, 8.965, 1.418 and 1.304, respectively. The ranges (in angstroms) for quartz, calcite, montmorillonite, Lost Hills and coal, respectively, are: 6–40 (average ~12), 15–50 (average ~25), 5–8 (average –6), 12–100 (average ~30), and 5–20 (average ~10). Macro-pore sizes estimated for the Lost Hill core and coal are on the order of several thousand angstroms in diameter. These data are needed to assess the behavior of CO_2 adsorption and its subsequent isotope partitioning during interaction with solids.

Model mass-balance isotope reaction calculations were conducted to assess the magnitude of both C and O isotope change in CO_2 as it reacts with calcite and water (see Figure 16). The calculations assume reaction in a closed system where CO_2 is allowed to react simultaneously with a HCO^-_3-brine and calcite. Equilibrium isotope fractionation is assumed in all calculations carried out for both 20° and 100°C. The results of these calculations are shown in Figure 16 where $\delta^{13}C$ (on the PDB scale) are plotted against the $\delta^{18}O$ (on the SMOW) of CO_2. The initial

CO_2 has been given values of 32 per mil and –36 per mil for O and C, respectively. The isotopic change in C and O are calculated for different scenarios where CO_2 is reacted with calcite and H_2O of varying initial composition. In all cases, the C isotope values of CO_2 increase because we allow it to react with calcite having a single initial enriched value (0 per mil). We see that, depending on whether the initial calcite and brine are enriched or slightly depleted in ^{18}O, the CO_2 isotopic trajectories can be quite different [i.e. one with increasing ^{18}O (trajectories moving to the upper right) versus those that decrease (trajectories moving to the upper left)]. Magnitudes of change along any given trajectory are controlled by initial isotopic compositions, temperature and the ratio of CO_2 to calcite+brine, examples of which are shown as open circles with their respective CO_2/calcite+H_2O oxygen and carbon mole ratios. These preliminary calculations indicate that by coupling the experimental partitioning data with measurements from real field tests, simple models may contribute to our understanding of how CO_2 migrates and what it encounters in the subsurface.

One sample of Lost Hills core (Chevron OB-7, 1461 feet—horizontal orientation) was subjected to a number of preliminary organic solvent extractions to assess what kinds of organic compounds dominate in this sample. Standard solvent extraction methods were employed (such as methylene chloride-methanol) to liberate select fractions of the organic compounds. Thermogravimetry (TGA), gas chromatography (GC) and gas chromatography-mass spectrometry (GC-MS) were used to analyze this sample. Up to 15 wt. % water was liberated from the sample during TGA analysis. GC and GC-MS analyses indicate that this particular core sample is rich in alkylated compounds, specifically alkylated cyclohexane rings, alkylated benzene rings, and alkylated tetrahydronaphthalene, along with naphthalenes and assorted steroids such as cholestane. Because the effect of hydrocarbons on isotopic partitioning involving CO_2 is so profound, we hope to use our understanding of the organic chemistry to design adsorption experiments where we utilize representative geologic materials (e.g., quartz, calcite) coated with end-member organic compounds common to the Lost Hills system to assess whether the sorption-isotope effect is compound-specific.

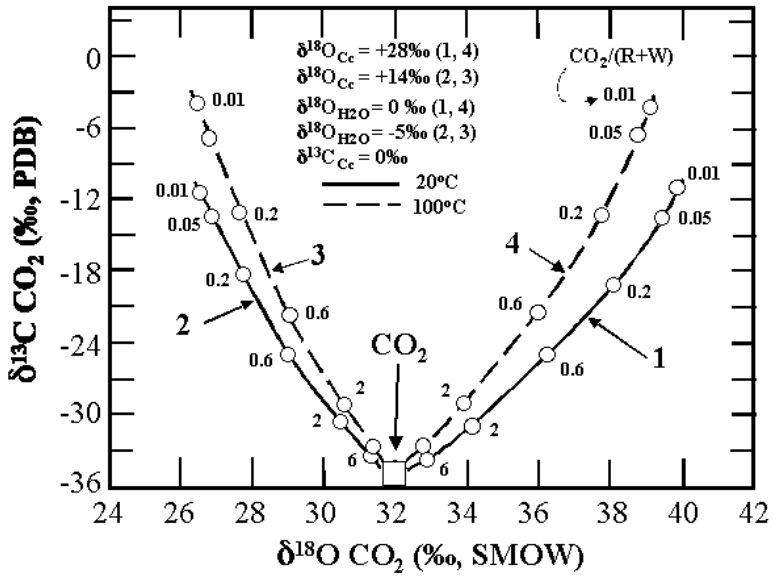

Figure 16. Results of mass-balance isotopic-reaction modeling.

Work Next Quarter: Efforts in the next quarter will focus on four main areas:

a) Continuation of core-gas-fluid isotope exchange experiments, emphasizing the role of changing surface area and organic compounds on the magnitude of partitioning
b) Complete CO_2 sorption-desorption experiments using Argonne Premium coals as well as Lost Hills core and mineral end-members, quartz, calcite, and montmorillonite
c) Initiation of a modeling effort using Geochemists Workbench to assess the magnitude of carbon and oxygen isotope partitioning during gas-brine-mineral reactions relevant to subsurface aquifer formation conditions.
d) Construction of a flow-through column apparatus and laboratory testing of the applied tracers using similar geological materials as in the isotopic-tracer experiments.

Task C: Enhance and Compare Simulation Models

Subtask C-1: Enhancement of numerical simulators for greenhouse gas sequestration in deep, unmineable coal seams.

Accomplishments:

- Testing of Schlumberger GeoQuest's coalbed methane (CBM) numerical simulator, ECLIPSE, was carried out using the first two sets of benchmark problems.
- Development of second generation, more complex, benchmark problems was initiated.
- Analytical solutions for multicomponent gas flow coupled with adsorption in coalbeds were developed.

Summary:

The goal of this subtask is to improve simulation models for capacity and performance assessment of CO_2 sequestration in deep, unmineable coal seams.

Work began with definition of the physical processes that ultimately should be included in coalbed methane (CBM) numerical simulators. Benchmark problems were then developed for testing and comparison of available CBM codes. The first problem set is a single-well test with CO_2 injection into a coal seam. The second set is an enhanced coalbed methane (ECBM) process with CO_2 injection in a 5-spot well pattern. A website was established to document the benchmark problems and to post solutions. Using the first two problem sets, testing of several codes including GCOMP, SIMEDII, STARS and GEM have been completed.

Progress this Quarter: Using the first two benchmark problem sets, Schlumberger GeoQuest's CBM numerical simulator, ECLIPSE, was tested. Agreement was reached with Advanced Resources International (ARI) to participate in the model comparison study using their CBM numerical simulator, COMET2. The contact is Scott Reeves in Houston, Texas, U.S.A.

ARC is working with TNO to set up two new sets of more complex numerical simulation benchmark problems. Problem Set 3 is the extension of Problem Set 2 but taking into account the effect of mixed gas diffusion between the coal matrix and the natural fracture system (dual porosity approach). Problem Set 4 is the extension of Problem Set 2 but taking into account the effect of stress on the permeability/porosity of the natural fracture system (Palmer & Mansoori model).

A report entitled "Modeling of Carbon Dioxide in Coalbed: Model Improvement," by David H. -S. Law, W.D. (Bill) Gunter and L.H.G. (Bert) van deer Meer was completed.

In a complementary effort, analytical solutions for multicomponent gas flow in coalbeds coupled with adsorption were developed. The system methane, nitrogen, and carbon dioxide were considered as an example.

Work Next Quarter: Testing of the first two problem sets using Schlumberger GeoQuest ECLIPSE will be completed. Benchmark Problem Sets 3 and 4 will be posted on the ARC website: http://www.arc.ab.ca/extranet/ecbm/ with user name: arcecbm and password: coal. Numerical results from COMET2 will be analyzed. Negotiations will take place with Burlington Resources for the release of field data from their CO_2-ECBM pilot for a problem set, which predicts N_2 and CO_2 breakthrough. Work will also continue on a completely generic formulation for multicomponent gas flow with adsorption where the behavior of an injection gas of any composition can be computed. A report is in preparation detailing the analytical solution method and showing example calculations.

Subtask C-2: Intercomparison of reservoir simulation models for oil, gas, and brine formations

Accomplishments:

- Information exchange continued with the ten groups in six countries who have committed to participating in the study, as well as with additional interested parties.

Summary:

The objective of this subtask is to stimulate the development of models for predicting, optimizing, and verifying CO_2 sequestration in oil, gas, and brine formations. The approach involves: (1) developing a set of benchmark problems, (2) soliciting and obtaining solutions for these problems, (3) holding workshops of industrial, academic, and laboratory researchers, and (4) publishing results.

To date, a set of light benchmark problems have been established. Processes encompassed by these problems include carbon sequestration with enhanced gas recovery, aquifer disposal of CO_2 (with geochemical interactions), hydro-mechanical coupled processes, and miscible and inmiscible displacement of oil by CO_2. Materials for the intercomparison study have been mailed out, and posted on the Web. A detailed report on study design and milestones as well as specifications for a first set of eight test problems was completed.

Progress this Quarter: Effort focused on providing information on the code intercomparison study to interested parties and maintaining contact with the ten groups (in six countries) who have committed their participation and are working on the test problems.

Some enhancements were made to in-house simulation codes in preparation for running the test problems.

Work Next Quarter: Simulation studies of test problems for the code intercomparison will be carried out, and enhanced and more realistic problem specifications will be developed. Interaction with the various participating groups will be maintained, including guidance and commentary on preliminary results.

Task D: Improve the Methodology and Information for Capacity Assessment

Accomplishments:

- An updated definition of formation storage capacity was developed that consists of the product of four factors: intrinsic capacity, a geometric capacity factor, a heterogeneity capacity factor, and porosity.
- The capacity of brine formations for storage of CO_2 at a Frio formation site near Baytown, Texas, was assessed using numerical simulation.

Summary:
The objectives of this task are to: (1) improve the methodology and information available for assessing the capacity of oil, gas, brine, and unmineable coal formations; and (2) provide realistic and quantitative data for construction of computer simulations that will provide more reliable sequestration capacity estimates.

As a preliminary step in performing capacity-assessment simulations in brine formations, mathematical models were developed to assess the relative contributions to total sequestration capacity from CO_2 (1) in the gas phase, (2) dissolved in the aqueous phase, and (3) in solid minerals. Capacity factors for the three different storage modes were defined as the equivalent gas saturations that would be required to store the same amount of CO_2. These capacity factors were partially evaluated through analytical estimates and numerical simulations. As a next step, the effect of formation geometry and heterogeneity has been included in the definition of an updated capacity factor.

The Texas Gulf Coast was targeted as an area from which a realistic data set could be generated for use in simulation of capacity in brine formation. Location and identifying information were compiled for large industrial CO_2 emitters and geologic data for the Frio and Oakville reservoirs were compiled. A realistic scenario for CO_2 injection into a brine formation was then designed for a site near Baytown, Texas.

Progress this Quarter: The new definition of capacity was developed to shift the focus from a mechanistic comparison of physical processes in an idealized geologic setting to a practical means of investigating how much of a complex geologic formation can actually be used for CO_2 sequestration. We construct capacity C as the product of four factors:

$$C = C_i \cdot C_g \cdot C_h \cdot \phi. \qquad (1)$$

C_i is intrinsic capacity, which is controlled by multiphase flow and transport phenomena; C_g is the geometric capacity factor, which is controlled by formation geometry; C_h is heterogeneity capacity factor, which is controlled by geologic variability; and ϕ is porosity, the fraction of void space within the formation. This formulation was found to be useful for investigating the different processes that influence C and for comparing this approach to that of other authors. In practice, however, one may not be able to separately calculate C_i, C_g, and C_h.

Intrinsic capacity C_i is defined as the fraction of pore space occupied by CO_2 assuming radial flow through a uniform medium. This is the setting for the original capacity definition, and the

analytical estimates previously developed still apply. C_i is the sum of gas and aqueous phase contributions, $C_i = C_{ig} + C_{il}$. For the gas phase,

$$C_{ig} \cong S_g, \tag{2}$$

where S_g is the average gas saturation behind the front (the small contribution of water vapor to S_g has been neglected).

For CO_2 dissolved in the aqueous phase,

$$C_{il} = S_l X_l^{CO2} \rho_l / \rho_g, \tag{3}$$

where S_l and X_l^{CO2} are the saturation and CO_2 mass fraction, respectively, averaged over the liquid (aqueous) phase behind the front, and ρ_l/ρ_g is the liquid/gas density ratio.

Geometric capacity factor C_g accounts for departures from the idealized radial flow geometry assumed for intrinsic capacity, such as partially penetrating injection wells, gravity segregation, and dipping formations with spill points. Figures 17a and 17b illustrate the effect of partial penetration and gravity on CO_2 plume development in a homogeneous medium.

Heterogeneity capacity factor C_h accounts for bypass flow arising from geologic heterogeneity, as illustrated in Figure 17c. This factor has been referred to as horizontal sweep efficiency in the petroleum literature.

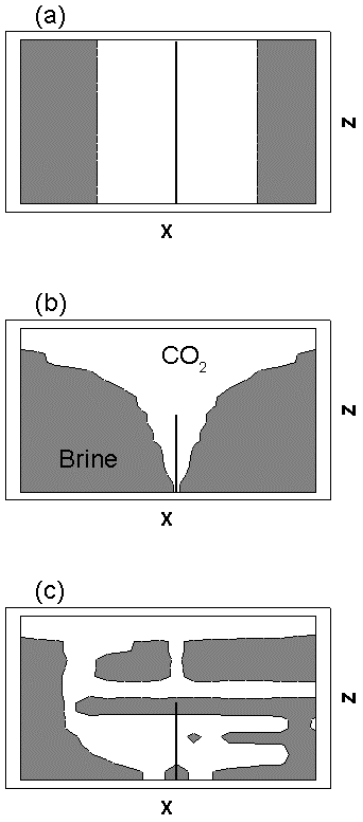

Figure 17. Schematic representations of CO_2 injection for (a) a uniform medium without gravity, (b) a uniform medium with gravity, and (c) a heterogeneous medium with gravity.

For nonradial flow or a heterogeneous medium, there may not be a single CO_2 front. We extend the definitions of C_{ig} and C_{il} given in Equations (2) and (3) to

$$C_{ig} \cdot C_g \cdot C_h = \langle S_g \rangle, \tag{4}$$

$$C_{il} \cdot C_g \cdot C_h = \langle S_l X_l^{CO2} \rho_l / \rho_g \rangle, \tag{5}$$

where <> identifies the region of space over which averages are taken. Examples of averaging regions include the volume of a natural CO_2 trap (defined by the distance from the injection well to a spill point or cap rock discontinuity), the volume of a targeted geologic formation, or some relevant unit volume (e.g., 1 km^3 around a power plant). Obviously, the choice of averaging region can have a large effect on the capacity value calculated, so it must be chosen carefully to ensure meaningful comparison of different scenarios.

The stage of CO_2 plume development at which capacity is calculated is also important. Averages may be taken when the boundary of the averaging region is first encountered or, alternatively, when quasi-steady flow conditions exist throughout the averaging region.

Numerical simulations of 20 years of CO_2 injection followed by 40 years of recovery were conducted for three cases: The heterogeneous 3D model shown in Figure 18 of the previous quarterly report (the base case), the same model with uniform hydrologic properties (to examine the effect of C_h), and a radial flow model with uniform properties and no gravity (to examine the effects of C_g and the constant pressure boundary).

Figure 18 shows a series of snapshots of the gas-phase CO_2 distribution during the 20-year injection period for the base case. The interplay of gravity and geological heterogeneity leads to a highly irregular CO_2 distribution.

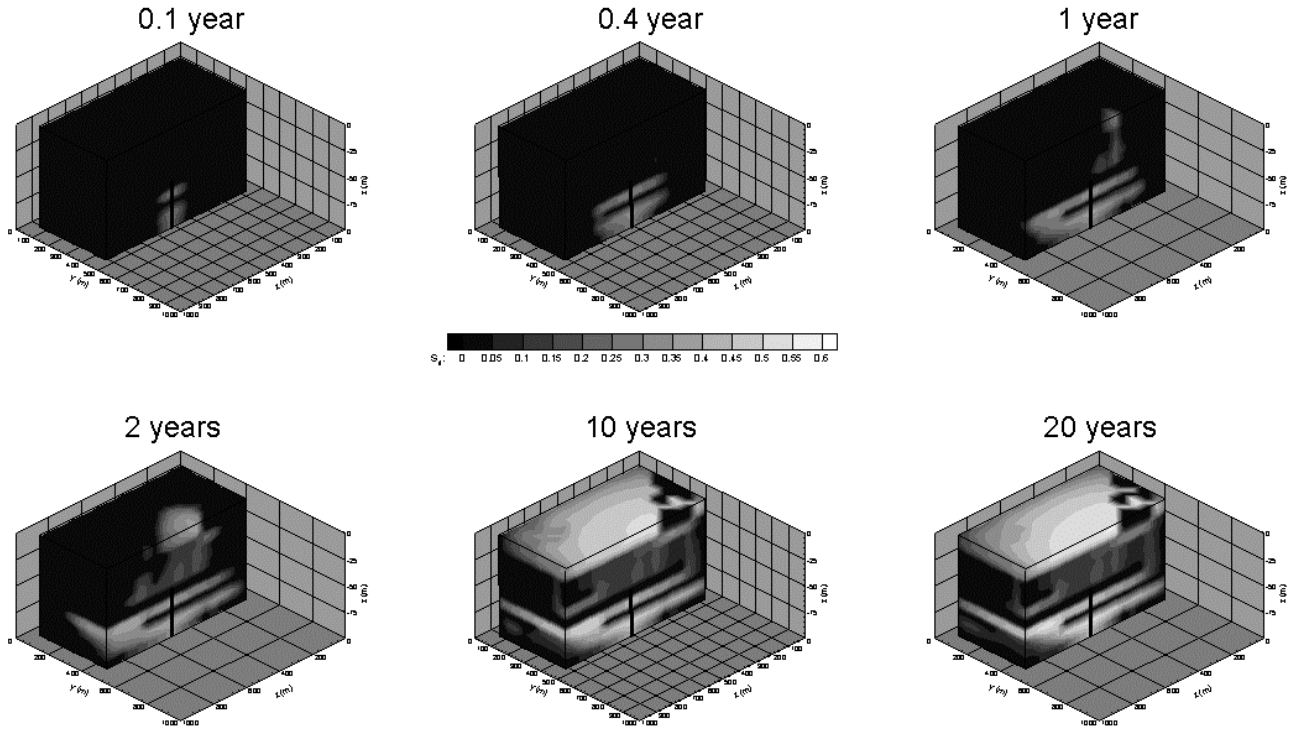

Figure 18. Snapshots of the gas-phase CO_2 distribution during the injection period for the base case.

Figure 19 shows the cumulative masses of CO_2 injected and in place during the 60-year simulation period. These masses are identical until the outer boundary (spill point) of the model is reached after about 1 year of injection. Quasi-steady flow conditions (approximately equal CO_2 masses injected into the well and leaving the model through the lateral boundaries) develop after about 10 years of injection. Throughout most of the injection period, the phase partitioning of CO_2 into liquid and gas phases remains relatively steady with about 15—20% of the CO_2 dissolved in the aqueous phase. However, after injection ends, the mass of CO_2 in the gas phase decreases (leakage out the lateral boundaries), whereas the mass of CO_2 dissolved in the aqueous phase increases slightly.

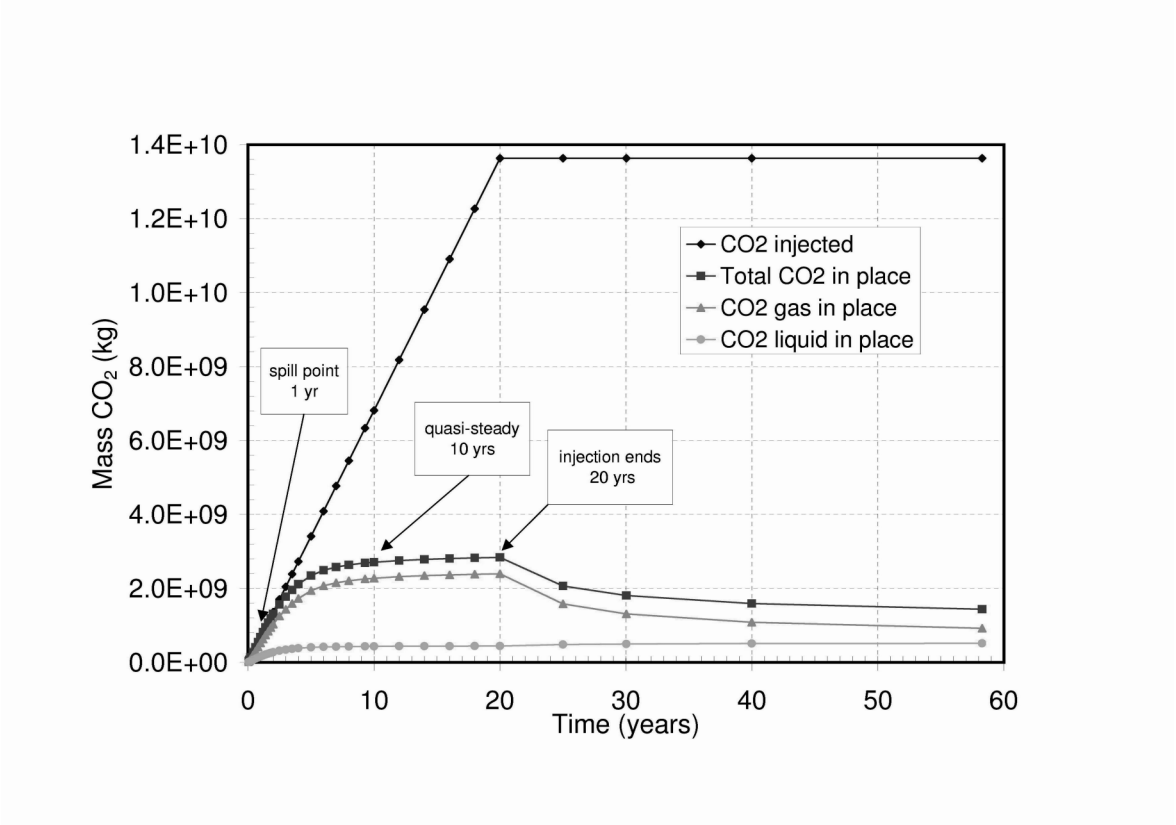

Figure 19. Cumulative CO_2 injected and in place for the heterogeneous 3D model (the base case).

In addition to the numerical simulation work, effort was also directed at locating a pilot site for injection of CO_2 into a brine formation. The Woodbine Formation of East Texas Basin was revisited. This sandstone is a close equivalent to the Utsiera Formation where CO_2 is now successfully injected. The Woodbine Formation has more than a Darcy permeability, very high sweep efficiency, is regionally pressure depleted, and is isolated from outcrop on all sides of the basin by faulting or angular nonconformaties. Large lignite-burning power plants release large volumes of CO_2 and are significant contributors to citizen and regulator concerns about air quality in the area. Potential reuse of the old Woodbine reservoirs as the fields go into decline are of interest to local stakeholders, and a CO_2 experiment would be well received. We are discussing the prospects for a field experiment with operators who have leases in the East Texas Field.

We began site-specific data collection for our Cedar Bayou Frio modeling experiment, including digitizing existing structure maps on several Frio horizons. We also collected logs from the Bureau of Economic Geology log library in preparation for cross section creation. We visited an operator with leases in the area (South Liberty and Goose Creek) and examined the existing geologic data to propose areas that might be prospects for field studies.

Sketches of the geologic setting in these three areas (East Texas Field woodbine, South Liberty, and Goose Creek) were prepared and distributed to the project team for comment. South Liberty and Goose Creek are fields associated with salt domes. The target intervals are highly compartmentalized by growth faulting and sandstones separated by shale seals. The Woodbine is relatively homogeneous sandstone that dips westward off the Sabine uplift. The top seal is the Austin Chalk. Well spacing in the old field is very close, and quality of cement jobs would be an issue included in the experiment.

Cost Summary:

	LBNL (Including subcontract to Stanford, TBEG, and ARC)	**LLNL**	**ORNL**
FY01 Funding + carryover	$507,000	$196,700	$194,900
Quarterly Cost	$181,700	$78,000	$65,080
FY01 Cumulative Cost	$353,500	$196,000	$154,280
Remaining Balance	$153,500	$700	$40,620